Antiproton Production in Relativistic Si-Nucleus Collisions

J. Barrette,[3] R. Bellwied,[6] P. Braun-Munzinger,[6] W. E. Cleland,[5] T. Cormier,[8] G. Dadusc,[6] G. David,[6] J. Dee,[6] G. E. Diebold,[9] O. Dietzsch,[7] E. Duek,[1] M. Fatyga,[1] D. Fox,[2] S. V. Greene,[9] J. V. Germani,[9] J. R. Hall,[4] T. K. Hemmick,[9] N. Herrmann,[6] R. W. Hogue,[1] B. Hong,[6] K. Jayananda,[5] D. Kraus,[5] B. S. Kumar,[9] R. Lacasse,[3] D. Lissauer,[1] W. J. Llope,[6] T. W. Ludlam,[1] R. Majka,[9] D. Makowiecki,[1] S. K. Mark,[3] J. T. Mitchell,[9] M. Muthuswamy,[6] E. O'Brien,[1] C. Pruneau,[3] F. S. Rotondo,[9] J. Sandweiss,[9] N. C. da Silva,[7] J. Simon-Gillo,[8] J. Slaughter,[9] U. Sonnadara,[5] J. Stachel,[6] H. Takai,[1] E. M. Takagui,[5] T. G. Throwe,[1] L. Waters,[6] Ch. Winter,[9] K. Wolf,[8] D. Wolfe,[4] C.L. Woody,[1] N. Xu,[6] Y. Zhang,[6] Z. Zhang,[5] and C. Zou[6]

(E814 Collaboration)

[1] *Brookhaven National Laboratory, Upton, New York 11973*
[2] *Los Alamos National Laboratory, Los Alamos, New Mexico 87545*
[3] *McGill University, Montreal, Canada H3A 2T8*
[4] *University of New Mexico, Albuquerque, New Mexico 87131*
[5] *University of Pittsburgh, Pittsburgh, Pennsylvania 15260*
[6] *State University of New York, Stony Brook, New York 11794*
[7] *Universidade de São Paulo, São Paulo, Brazil*
[8] *Texas A&M University, College Station, Texas 77843*
[9] *Yale University, New Haven, Connecticut 06511*

(Received 3 September 1992)

We have measured antiproton production cross sections as functions of centrality in collisions of 14.6 GeV/c per nucleon ^{28}Si ions with targets of Al, Cu, and Pb. For all targets, the antiproton yields increase linearly with the number of projectile nucleons that have interacted, and show little target dependence. We discuss the implications of this result on the production and absorption of antiprotons within the nuclear medium.

PACS numbers: 25.75.+r

Nucleus-nucleus collisions at relativistic energies are an effective way to create states of hot and dense nuclear matter, and perhaps quark matter in the laboratory. Antiprotons ($\bar{p}$) are of particular interest in such studies because their distributions are expected to be influenced by the baryon densities of the systems produced in these collisions [1]. Antiprotons have large annihilation cross sections in baryon rich environments. Their survival probability could be used to understand both the collision environment and the $\bar{p}$ formation times. In the event of quark-gluon plasma formation, theoretical calculations predict the enhanced production of antiprotons [2]. Other calculations suggest that even without plasma formation $\bar{p}$ production is enhanced in high energy heavy ion collisions [3–5]. We describe herein measurements of antiproton production at midrapidities, and small transverse momenta in collisions of 14.6 GeV/c per nucleon ^{28}Si ions impinging on Al, Cu, and Pb targets. We have measured the yields per event as functions of transverse energy (E_t) [6], and forward energy (E_{ZD}) to assess the possible enhanced production and the magnitude of absorption of the antiprotons within the collision environment, as functions of centrality (in essence the impact parameter of the collision). Our measurements are unique in their simultaneous exploration of the collision geometry and target mass dependence of $\bar{p}$ production.

The experiment used the E814 apparatus [7, 8] at the Brookhaven National Laboratory Alternating Gradient Synchrotron (AGS) facility. It has detectors for global event characterization and a forward spectrometer accepting particles emitted within a rectangular aperture ($\Delta\theta_x = 37.6$ mrad and $\Delta\theta_y = 24.1$ mrad) centered on the beam axis. The detectors surrounding the target consist of a silicon pad multiplicity detector covering in pseudorapidity η the range $0.9 < \eta < 3.9$, a NaI target calorimeter and a scintillator paddle array lining its inside covering $-0.5 < \eta < 0.8$, and a Pb-scintillator sampling calorimeter covering $0.9 < \eta < 3.9$. The forward spectrometer consists of two dipole magnets, three tracking chambers, a scintillator wall, and a U-Cu-scintillator sampling calorimeter. The centrality of each event can be determined by independent measurements of E_t in the target and participant calorimeters, charged particle multiplicity measured in the silicon detector, and E_{ZD} measured by the calorimeters in the spectrometer. The Al, Cu, and Pb targets used in the measurement had thicknesses of 2.6, 5.6, and 11.3 g/cm^2, respectively, corresponding to $\sim 10\%$ of a ^{28}Si interaction length. The number of interactions sampled was $\sim 3.3 \times 10^7$ for each target.

Interactions in the target were selected by a pretrigger defined by a valid beam particle, in coincidence with a minimum of 25 hits in the multiplicity detector and 5 in the scintillator paddles, or 25 hits in the multiplicity detector and 5 GeV of E_t in the participant calorimeter. The magnetic field in the spectrometer ensured that most

of the particles striking the trigger region of the scintillator hodoscopes were negatively charged. The times of flight measured by this subset of scintillators were examined to establish if a particle of interest traversed the spectrometer. This selection was designed to enhance detection of those events containing $\overline{p}$ candidates with y within ± 0.4 of the nucleon-nucleon center of mass rapidity, $y_{NN} = 1.72$. Such antiprotons will reach the trigger region between 3 and 30 ns later than particles traveling at the velocity of light. The scintillator hodoscope is located 31 m downstream of the target and provides a time-of-flight determination at the trigger level with a resolution, after slewing corrections, of 600 ps. The off-line time-of-flight resolution was measured to be 480 ps.

The analysis of the data proceeds with the identification of valid tracks through the spectrometer which satisfy the kinematic requirements of $\overline{p}$ candidates. Two drift chambers and a pad chamber measure the momenta of tracks with a resolution, for a total field integral of 0.40 T m, of $\Delta p/p^2 \leq 1 \times 10^{-2}$ $(\mathrm{GeV}/c)^{-1}$. Two pad chambers and the forward scintillator wall provide position measurements perpendicular to the magnetic bend plane. Accepted tracks are required to have registered on all of the planes. The efficiency of each pad chamber and of the forward scintillator wall was determined experimentally to be ~90%. The drift chambers operate at efficiencies of ~ 100%. In addition, the magnitude of the charge of the detected particle is required to be 1 (× electron charge) as determined by the pulse height measured in the forward scintillator wall. Also, the measured momenta of the particles were required to be consistent within $\pm 3\sigma$ with the energy measured by the calorimeter for the same tracks. The net efficiency in the pattern recognition and track reconstruction including all of these effects is 58%.

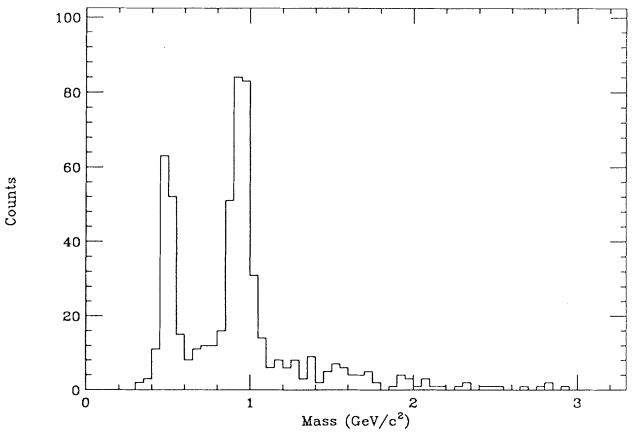

FIG. 1. A plot of the reconstructed masses of negatively charged particles detected in the spectrometer acceptance for Si+Pb interactions. The trigger conditions are described in the text.

Figure 1 is a plot of the mass of negatively charged particles as determined from measurements in the forward spectrometer for Si+Pb interactions under the trigger conditions described above. Antiprotons are selected by requiring a reconstructed mass to be between 0.7 and 1.18 GeV/c^2. The background under the peak was estimated from fits to the data to be 29%, 22%, and 22% for the Al, Cu, and Pb targets, respectively. The total number of antiprotons thus selected with background subtracted is 163, 235, and 246, respectively, for the three targets.

Figure 2(b) is a plot of the acceptance ϵ of the spectrometer for antiprotons shown as a function of transverse momentum p_t. It includes the effects of the spectrometer entrance aperture, magnetic field, and the losses of flux owing to interactions of the antiprotons with the detector elements, and was obtained in a Monte Carlo simulation of the apparatus using the GEANT program [9]. Trigger biases and multiple scattering are not accounted for in these plots, and are discussed below.

Our measured pretrigger cross section for the Pb target was 3650 mb. For the Al and Cu targets it was only 1320 and 2016 mb, respectively—20% and 10% smaller than the corresponding calculated geometric cross sections. This is because of pretrigger inefficiencies for the most peripheral collisions, and results in an estimated loss of 1%, and 6% of the antiprotons for the Cu and Al targets, respectively. There is also a loss of 7% of antiprotons for all three targets from the 600 ps resolution of the time-of-flight trigger, representing 35% of the yield in the highest rapidity bin ($1.9 < y < 2.1$). In addition,

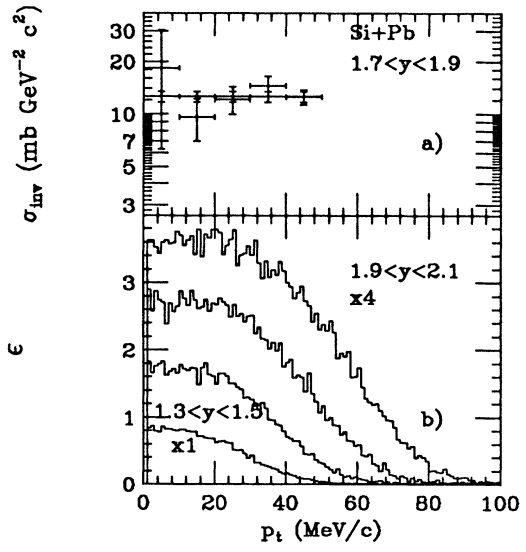

FIG. 2. (a) The invariant cross section $\sigma_{\mathrm{inv}} = \frac{1}{2\pi p_t}\frac{d^2\sigma}{dy dp_t}$ (mb GeV^{-2} c^2), and (b) the acceptance, ϵ, of the E814 forward spectrometer plotted as functions of transverse momentum. The four curves are for rapidity bins of width 0.2, starting at $y = 1.3$, and have been scaled by factors of 1, 2, 3, and 4.

we estimate that there is a further loss of yield of 10% (50% in the highest rapidity bin) owing to systematic uncertainties in the calibration of the time-of-flight trigger. This has been corrected for based on an observed asymmetry in the rapidity dependence of the invariant cross section for the Si+Al interactions. These corrections result in a large uncertainty only for the data in the highest rapidity bin, and not for the rapidity-integrated yield.

The $\overline{p}$ yields per interaction within the spectrometer acceptance, averaged over impact parameter, are $(1.1\pm0.1)\times10^{-5}$, $(1.5\pm0.2)\times10^{-5}$, and $(1.6\pm0.2)\times10^{-5}$ for the Al, Cu, and Pb targets, respectively. These numbers are corrected for all of the effects described above. Our measured yield ratios of antiprotons from Al and Cu targets relative to Pb are 0.69 ± 0.08 and 0.94 ± 0.1, and agree with the measurements of two other AGS experiments, E802 and E858. The integrated ratio of the yields measured by E802 [10, 11] in the rapidity range $1.1 < y < 1.7$ and for $p_t > 0.3$ is 0.75 ± 0.15 for the Al target relative to Au. E858 reports 0.69 ± 0.14 and 0.82 ± 0.16 for the Al and Cu targets, respectively, relative to Au, at $p_t = 0$ and y=1.7 [12].

Figure 2(a) plots, as a function of p_t, our measurement of the invariant cross section for antiprotons, averaged over impact parameter, for Si+Pb interactions. It is constant, within uncertainties, over the p_t interval covered. For the Pb target, the resolution in p_t is $\Delta p_t \sim 20$ MeV/c, and is dominated by multiple scattering. Table I lists the invariant cross section at p_t=0 for the three targets, obtained from fits to the data. The points considered in the fit were those for which the acceptance shown in Fig. 2(b) exceeded 0.33. The cross sections are a factor of $\sim$ 2 below those obtained by extrapolations of the measurements of E802 [10] to $p_t = 0$. At the same time, our numbers are a factor of $\sim$2 higher than measurements of E858 [12] made in a similar region of y and p_t. The discrepancy with E858 is as yet unresolved. Notwithstanding the fact that there are uncertainties associated with these comparisons, it is interesting to note that these numbers may indicate the presence of a low p_t suppression in the yield of antiprotons.

A unique aspect of this experiment is our ability to explore the impact parameter dependence of $\overline{p}$ production. For the sake of brevity, we focus on the forward energy (E_{ZD}) as a measurement of centrality. A reliable measure of E_{ZD} for each event can be obtained by summing the energy deposited in five calorimeter modules in the forward calorimeter wall. The calorimeter measures energy with a resolution of $\sigma_E/E = 0.6/E^{1/2}$ (E in GeV). The E_{ZD} measurement enables us to quantify the number of projectile nucleons that have interacted. The dominant contribution to E_{ZD} is from beam rapidity fragments. There is a small additional contribution that comes from particles produced by the part of the projectile that has interacted. We can estimate this from our previous measurements [7, 8] to be a few GeV only. From this E_{ZD} measurement we, therefore, determine the number of projectile nucleons that have interacted, $N_{\rm int}$, as equal to $28 - E_{ZD}/13.6$ (E_{ZD} in GeV). We can then explore the production of antiprotons as a function of $N_{\rm int}$. Figures 3(a)–3(c) show the $\overline{p}$ yield per interaction at a given centrality plotted as functions of $N_{\rm int}$. These numbers were obtained by dividing the $d\sigma/dN_{\rm int}$ distributions of events containing antiprotons by the corresponding pretrigger distributions. It is remarkable how similar the data are for the three targets.

Previous measurements of $\overline{p}$ yields in $p+p$, p+Be, and p+Pb collisions at 18.8 GeV/c have established that the yield per interaction changes by only 30% as a function of target mass [13]. The $p + p \rightarrow \overline{p}$ production cross section is strongly energy dependent for energies $\sqrt{s} < 20$ GeV. Considering this, the p+nucleus data seem to indicate the dominance of $\overline{p}$ production in *first* collisions,

TABLE I. $\frac{1}{2\pi p_t}\frac{d^2\sigma}{dy dp_t}$ (mb GeV^{-2} c^2) at $p_t = 0$ for the Pb, Cu, and Al targets as a function of rapidity. The numbers have been corrected for background, and for detection and analysis efficiencies.

	Rapidity			
Target	1.3–1.5	1.5–1.7	1.7–1.9	1.9–2.1
Al	3.0 ± 1.0	3.5 ± 0.6	3.3 ± 0.6	3.0 ± 1.0
Cu	5.8 ± 2.0	7.1 ± 1.0	7.0 ± 1.0	5.2 ± 1.5
Pb	7.2 ± 3.1	13.0 ± 2.5	12.0 ± 1.3	8.2 ± 1.5

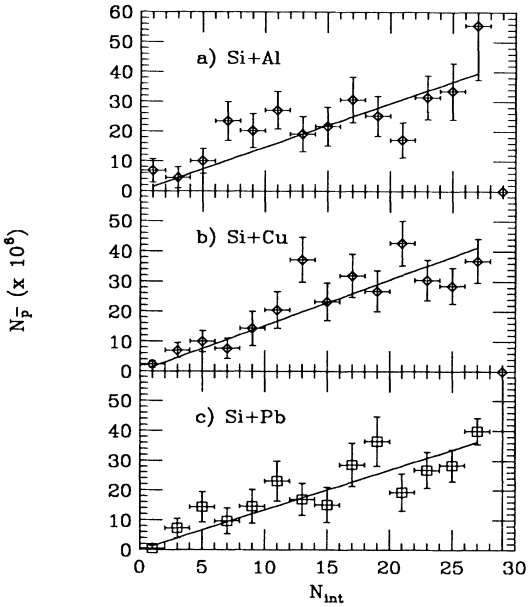

FIG. 3. The number of antiprotons produced per nucleus-nucleus interaction, $N_{\overline{p}}$, at a given centrality, plotted as functions of the number of projectile nucleons that have interacted, $N_{\rm int}$. The panels are (a) Si+Al, (b) Si+Cu, and (c) Si+Pb interactions, respectively. The lines are fits to the data using first order polynomials.

those in which projectile and target nucleons are interacting for the first time. Such an assumption, if applicable to nucleus-nucleus collisions, would imply that $\overline{p}$ yields should increase linearly with $N_{\rm int}$, since $N_{\rm int} \propto N_f$, the number of *first* collisions [14]. Furthermore, should some or most of the produced antiprotons be annihilated, this would be evident in the smallest impact parameter or highest $N_{\rm int}$ events. To test this, fits to the data were performed and are shown as solid curves in Figs. 3(a)–3(c). The curves are constrained to pass through the origin, implying no $\overline{p}$ production in the absence of nuclear interactions. Their slopes are $(1.5 \pm 0.2) \times 10^{-6}$, $(1.5 \pm 0.2) \times 10^{-6}$, and $(1.3 \pm 0.2) \times 10^{-6}$ for the Al, Cu, and Pb targets, respectively, and are consistent with the impact parameter averaged results discussed below, if scaled by a factor of 1.95, the ratio of the mean number of first collisions $\langle N_f \rangle$ to the mean number of interacting nucleons $\langle N_{\rm int} \rangle$ [14]. Unexpectedly, the data show no significant deviation from a straight line, and furthermore, there is little target dependence of the fitted slope parameters.

Nucleus-nucleus collision models like Venus and Fritiof do not describe the magnitude and trends seen in the $\overline{p}$ data [10]. On the other hand, relativistic quantum molecular dynamics (RQMD) calculations reproduce the E802 results, and are therefore expected to overpredict our data [3]. In a simple model we can use $p+p$ data to estimate the expected mimimum-bias $\overline{p}$ yields in nucleus-nucleus collisions, neglecting the effects of absorption, or multistep production. In a Monte Carlo calculation we generate $(1.2 \pm 0.3) \times 10^{-3}$ antiprotons per $p+p$ interaction. This number was obtained by extrapolating downwards to an energy of 14.6 GeV the $\overline{p}$ yields measured in $p+p$ collisions at higher energies [15]. The antiprotons are generated in a distribution of the following functional form, $dN/dp_t dy \propto p_t e^{-m_t/B} e^{-(y-y_0)^2/2\sigma_y^2}$, where $m_t = \sqrt{p_t^2 + m^2}$ and m is the mass of the $\overline{p}$. We used $\sigma_y = 0.5$, $y_0 = 1.72$, and $B = 0.141$ GeV, consistent with other measurements at AGS energies [10–12]. The antiprotons are then propagated through the E814 spectrometer, using GEANT, to determine the fraction that will be detected. We estimate that $(5.2 \pm 1.3) \times 10^{-6}$ antiprotons should be seen per *first* collision in the spectrometer. The mean numbers of *first* collisions, $\langle N_f \rangle$, has been calculated to be 3.5, 4.6, and 6.3, respectively, for Si ions interacting with Al, Cu, and Pb targets [14]. Hence, using our measured $\overline{p}$ yields per interaction, we determine the $\overline{p}$ yields per *first* collision in our apparatus to be $(3.1 \pm 0.3) \times 10^{-6}$, $(3.2 \pm 0.4) \times 10^{-6}$, and $(2.5 \pm 0.4) \times 10^{-6}$, respectively. The measured $\overline{p}$ yield is thus a factor of 1.7–2.1 smaller than expected for production in first chance collisions. However, the fact that the measured yields are approximately independent of target, together with the linear behavior displayed in Fig. 3, rules out an explanation of our data in terms of a combination of first chance production followed by absorption.

This leaves the following interpretations. Some models suggest that multistep effects are very important in determining the extent of $\overline{p}$ production in nucleus-nucleus collisions [3–5]. It is then the subtle interplay between increased $\overline{p}$ production and increased $\overline{p}$ absorption in this collision environment that can produce the surprisingly small target and centrality dependence seen in our measurements. On the other hand, in the model ARC the $\overline{p}$ production cross sections are not enhanced, but in-medium annihilation is suppressed because of the importance of three body interactions in dense nuclear media [16]. Our data should provide a stringent test of, and hopefully differentiate between, these two scenarios. In summary, the $\overline{p}$ yield per *first* collision, either determined as an average over impact parameter (minimum bias) or observed at different impact parameters (experimentally determined by measurements of forward energy) is independent of target and centrality. Irrespective of what the models have to say, this result is surprising, and demonstrates that the nucleus-nucleus collision environment is very unusual and a lot more interesting than a simple superposition of nucleon-nucleon collisions.

We thank the AGS staff, and Dr. H. Brown for providing us with beam, and J. Sondericker III and R. Hutter for technical support. This work was supported in part by the U.S. DOE, the NSF, NSERC, Canada, and CNPq, Brazil.

[1] S. Gavin, M. Gyulassy, M. Plumer, and R. Venugopalan, Phys. Lett. B **234**, 175 (1990), and references therein.
[2] C.M. Ko and X. Ge, Phys. Lett. B **205**, 195 (1988); K.S. Lee, M.J. Rhoades-Brown, and U. Heinz, Phys. Rev. C **37**, 1452 (1988); P. Koch and C. Dover, Phys. Rev. C **40**, 145 (1989); D.H. Rischke *et al.*, Phys. Rev. D **41**, 111 (1990).
[3] A. Jahns, H. Stöcker, W. Greiner, and H. Sorge, Phys. Rev. Lett. **68**, 2895 (1992).
[4] G. Batko, W. Cassing, U. Mosel, K. Niita, and Gy. Wolf, Phys. Lett. B **256**, 331 (1991).
[5] J. Schaffner, I.N. Mishustin, L.M. Satarov, H. Stöcker, and W. Greiner, Z. Phys. A **341**, 47 (1991).
[6] S.V. Greene, Ph.D. thesis, Yale University, 1992; S.V. Greene *et al.*, Nucl. Phys. **A544**, 599c (1992).
[7] E814, J. Barrette *et al.*, Phys. Rev. Lett. **64**, 1219 (1990).
[8] E814, J. Barrette *et al.*, Phys. Rev. C **45**, 819 (1992).
[9] GEANT, Version 3.14, R. Brun *et al.*, CERN Data Handling Division Report No. DD/EE/84-1 (unpublished).
[10] J. Costales, Ph.D. thesis, MIT, 1991.
[11] E802, T. Abbott *et al.*, Phys. Lett. B **271**, 447 (1991).
[12] E858, M. Aoki *et al.*, Phys. Rev Lett. **69**, 2345 (1992).
[13] D. Dekkers *et al.*, Phys. Rev. **137**, B962 (1965).
[14] B. Shiva Kumar, S.V. Greene, and J.T. Mitchell, Yale Report No. 40609-1092 (unpublished).
[15] J.V. Allaby *et al.*, CERN Report No. 70-12, 1970 (unpublished); T. Eichten *et al.*, Nucl. Phys. **B44**, 333 (1972); U.Amaldi *et al.*, Nucl. Phys. **B86**, 403 (1975).
[16] S.H. Kahana, Y. Pang, T. Schlagel, and C.B. Dover, Report No. BNL-48267, 1992 (unpublished).